Applied Thermal Engineering 237 (2024) 121529

Contents lists available at ScienceDirect

Applied Thermal Engineering

journal homepage: www.elsevier.com/locate/apthermeng

Research Paper

Pure hydrogen gas production in a coal supercritical water gasification system with CO_2 as transporting medium

Weizuo Wang [1], Qiuyang Zhao [1], Bingru Lu, Jinwen Shi, Hui Jin [*]

State Key Laboratory of Multiphase Flow in Power Engineering (SKLMF), Xi'an Jiaotong University, 28 Xianning West Road, Xi'an 710049, Shaanxi, China

ARTICLE INFO

Keywords:
Supercritical water gasification system
CO_2-transporting system
Coal utilization technology

ABSTRACT

Supercritical water gasification (SCWG) technology was a clean coal conversion and utilization technology, which could decompose low-grade coal into gaseous products and make efficient and clean use of them. However, system with H_2O transporting had much energy consumption on heating transporting medium and side reactions at heating process would weaken the gasification effect. Considering the advantages of low critical point and low specific heat capacity of CO_2, and the precedent of CO_2 as a transport medium in non-supercritical systems, CO_2 was expected to become a transport medium in supercritical water gasification systems and to achieve the goal of improving the gasification effect of heating process and reducing energy consumption. A supercritical water coal gasification system of was established with lignite as raw material in this paper. Production yields of gasification with CO_2 as the transporting medium at different working conditions were investigated. CO_2 and H_2O were used as the transporting medium of the system, contrastively. Compared with H_2O-transporting system, production of H_2 and CO_2 in CO_2-transporting system decreased while that of CH_4 and CO increased as well. Furthermore, both energy and exergy efficiency of CO_2-transporting system were higher than that of H_2O-transporting system. The result proved the superiority of CO_2 as the transport medium of supercritical water gasification system.

1. Introduction

With the development of society, energy demand and consumption are increasing. The current world energy structure is still dominated by oil, natural gas and coal. Coal is the most abundant fossil energy in the world. 46.1 % of the world's coal was produced in China in 2016 [1]. In China, India and some other countries, coals were widely used in metallurgy, chemical industry and power generation, especially the power generation [2–4]. 98% of the electricity in Poland came from hard coal and lignite [4].

As one of the major sources of global electricity, coal-fired power generation consumed about half of coal production in China [5]. However, the coal-fired power station caused much pollution in power generation. The insufficient combustion and energy grade of combustion led to low energy and exergy efficiency. Moreover, N and S atoms in the coals were also transformed into NO_X and SO_X [6,7]. Coal utilization technology was proposed to reduce the pollution and to rise the efficiency [8,9].

Supercritical water gasification was one of the coal utilization technologies with high efficiency [10,11]. At high temperature and pressure of water environment, complex organic feedstock such as coals was decomposed into H_2, CO_2 and other products such as CH_4, CO, oil and ash [12]. Water in supercritical phase not only played as a source of hydrogen and free radicals [13], but behaved like a catalyst as well [14], which led to the single-phase reaction environment in the reactor [15]. Moreover, supercritical water was a desirable reaction medium which could enhance mass transfer, prevent coke formation and avoid catalyst poisoning [16,17]. In order to avoid the introduction of other substances, water was generally used as the transporting medium to move the feedstock in previous supercritical researches and it could avoid the costly feedstock de-watering or drying [15]. In previous studies, many researchers investigated the energy and exergy of their own gasification system with H_2O transporting. Chen et al. did the thermodynamic, environmental analysis and comprehensive evaluation to obtain the optimal conditions [18]. A power generation system with integrated coal supercritical water gasification was established, in which coal-water-slurry concentration and the outlet pressure of the supercritical turbine were studied in another research [19]. Nurdiawati et al. established a novel system to produce H_2 from microalgae efficiently [20].

* Corresponding author.
E-mail address: jinhui@mail.xjtu.edu.cn (H. Jin).
[1] Equal contributions.

https://doi.org/10.1016/j.applthermaleng.2023.121529
Received 13 April 2023; Received in revised form 10 August 2023; Accepted 5 September 2023
Available online 6 September 2023

Nomenclature

En	Energy
Ex	Exergy
HE	Hydrogen conversion rate
LHV	Low heating value
M	Molecular weight
Mr	Mass percent of element
m	Mass flow
P	Power
PSA	Pressure swing adsorption
Q	Quantity of heat
SCWG	Supercritical water gasification
y	Yield

Greek symbols

η	Efficiency
ΔH	Endothermic quantity
ΔH_f^0	Standard molar enthalpy of formation
ω	Mass fraction

Subscripts

ad	Air drying base
en	Energy
ex	Exergy
H_2, CH_4, CO, CO_2	The name of the products
X	The name of product X
x,y,z	The name of sample $C_xH_yO_z$

The Achilles' heel was that side reactions at low temperature made the material react with water in temperature rising process. These side reactions were not conducive to the gasification reaction production and should be weakened [21]. Meanwhile, much heat was consumed in this process [22]. Mu et al. considered coal water slurry concentration as the key factor in supercritical gasification and believed the heating of water was the maximum exergy [23]. And our group showed that much heat was input into the system in gasification reactor [24]. A part of heat input was used to heat the transporting medium. Some researchers tried to increase the heating rate and reduce the resistance time of heating process [25,26], but reports on changing transporting medium were few.

On the other hand, supercritical CO_2 was also used as particle transporting medium [27]. He et al. added solid particles into the supercritical CO_2 to erode hard rocks and cut metals [28]; Sun et al. derived equilibrium flow rate model of proppant-carrying flow of supercritical CO_2 [29]; Hou et al. proposed an evaluation method to estimate the supercritical CO_2 thickening result for particle transporting [30]. Supercritical CO_2 showed good characteristics in pneumatic conveying in these researches. Compared with water, CO_2 had low critical point (31.3 °C and 7.38 MPa) [31] and low specific heat capacity [32], which meant CO_2 could cross the large specific heat region. Side reactions at low temperature were inhibited and the conversion rate of feedstock was high. Therefore, it was expected to inhibit side reactions and reduce the energy consumption if the transporting medium was changed to CO_2.

Based on these goals, a system of supercritical gasification was established in this paper. Gas production at different temperature, pressure and feedstock concentration (the ratio of H_2O, CO_2 and sample) was investigated to show the influence of factors. In addition, influence of these factors on the system energy and exergy analysis was also researched.

2. Materials and methods

2.1. Materials

The Yimin lignite from China was used in this paper, the same to the raw material in previous research [33]. The elemental and proximate analysis was shown in Table 1. It was obviously the elements of N and S contained no more than 1 wt% and the influence of these elements could be ignored to simplify the model.

2.2. Structure of system

Fig. 1 showed the structure of gasification system. It could be divided into four modules, the supercritical water module with water tank, pump, regenerator and preheater (blue pipe), the feedstock module with CO_2 tank, compressor and coal bunker (yellow pipe), the reaction module with gasification reactor, regenerator and valve (red pipe), the separation and purification module with separator, pressure swing adsorption (PSA) absorbers, high-purity H_2 tank and fuel tank (purple pipe). Moreover, a similar system was established in which H_2O was used as the transporting medium. In this H_2O-transporting system, CO_2 tank and compressor in the feedstock module were replaced by H_2O tank and pump.

Water from the water tank was pressurized by pump and heated by regenerator and preheater in the supercritical water module. Lignite was mixed with high-pressure CO_2 in the feedstock module. Productions in gasification reactor were calculated based on the lowest Gibbs free energy. The products and supercritical water output from the gasification reactor were cooled down and depressurized in regenerator and valve. In the separation and purification module, water was separated by separator and about 20 % of H_2 was purified by PSA module and stored in high-purity H_2 tank. H_2 could be separated from other gaseous production in PSA module and the purity of H_2 reached 99.99% [34,35].

2.3. Measurement parameters

The mass flow and mole flow of the products were considered the production of each product. The yield was considered as the production per kilogram of lignite. The yield of product X could be calculated as follow:

$$y_X = \frac{n_X}{m_{sample}} * 100\% \quad (1)$$

Reaction heat equaled the enthalpy difference between products and reactants at the reaction condition.

$$Q = \sum_{reactant} H - \sum_{product} H \quad (2)$$

Table 1
The elemental and proximate analysis of Yimin lignite.

Feedstock	Elemental analysis/ wt%				Proximate analysis/ wt%					Lower heating value/ MJ·kg^{-1}
Yimin lignite	C_{ad}	H_{ad}	N_{ad}	S_{ad}	O_{ad} *	M_{ad}	A_{ad}	V_{ad}	FC_{ad}	17.74
	40.50	3.25	0.57	0.19	21.43	18.42	15.64	32.21	33.73	

*: By difference; ad: air drying base; M: moisture, A: ash, V: volatile matter; FC: fixed carbon.

The hydrogen conversion rate (HE) was calculated as the quotient between hydrogen in products and hydrogen in feedstock.

$$HE = \frac{m_{H_2} + \frac{1}{4}m_{CH_4}}{m_{sample} * \omega_H} * 100\% \quad (3)$$

Energy and exergy efficiency was defined as the quotient of the output and input, as follow:

$$\eta_{En} = \frac{En_{Products}}{P_{Compressor} + Q_{input} + En_{Sample}} * 100\% \quad (4)$$

$$\eta_{Ex} = \frac{Exergy_{Products}}{P_{Compressor} + \int\left(1 - \frac{T_0}{T}\right)\delta Q + Ex_{Sample}} * 100\% \quad (5)$$

3. Results and discussion

3.1. Calculation of reaction heat

Without the influence of N and S elements, the sample of the research was defined as $C_xH_yO_z$, whose lower heating value at standard condition (25 °C and 0.1 MPa) could be calculated by Mendeleev's formula or measured by experiment. Thermochemical equation of gasification and its heat absorption were all calculated. The derivation process was as follow.

The main reactions were shown in (6) to (8) [36–38]. The steam reforming reaction was the most crucial and assumed to be completely shifted to the right side due to plenty of H_2O input into the reactor [37].

Steam reforming reaction:

$$C_xH_yO_z(s) + (2x - z)\ H_2O(g) \rightarrow xCO_2(g) + (2x + \frac{y}{2} - z)H_2(g) \quad (6)$$

Water-gas shift reaction:

$$CO(g) + H_2O(l) \rightarrow CO_2(g) + H_2(g) \quad (7)$$

Methanation reaction:

$$CO(g) + 3H_2(g) \rightarrow CH_4(g) + H_2O(l) \quad (8)$$

The relative molecular mass of the sample and mass fraction of each element was shown in (9) to (12).

$$M = (12x + y + 16z)\ g/mol \quad (9)$$

$$Mr_C = \frac{12x}{M} * 100\backslash\% \quad (10)$$

$$Mr_H = \frac{y}{M} * 100\backslash\% \quad (11)$$

$$Mr_O = \frac{16z}{M} * 100\backslash\% \quad (12)$$

The Lower heating value of the sample was calculated by Mendeleev's formula, shown in (13).

$$LHV = (339 * Mr_C * 100 + 1030 * Mr_H * 100 - 109 * Mr_o * 100)\ kJ/kg \quad (13)$$

Thermochemical equation of its complete combustion was shown in (14).

$$C_xH_yO_z(s) + (x + \frac{y}{4} - \frac{z}{2})\ O_2(g) \rightarrow xCO_2(g) + \frac{y}{2}H_2O(l)$$

$$\Delta H = LHV * M = (406.8\ x + 103\ y - 174.4\ z)\ kJ/mol \quad (14)$$

The enthalpy formation of the sample could be calculated with this equation.

$$\begin{aligned}\Delta H_f^0 &= [-(393.51 + 12 * LHV)\ x - (142.92 + LHV)\ y\ kJ/mol - (16 * LHV)z]kJ/mol \\ &= (-800.31\ x - 245.92y + 174.4z)\ kJ/mol\end{aligned} \quad (15)$$

So the thermochemical equation of gasification reaction at standard condition was shown in (16).

$$\begin{aligned}C_xH_yO_z(s) + \frac{4x - y - 4z + 2a + 4b}{6} H_2O(l) &\xrightarrow{25\ ^oC;\ 0.1\ MPa} aH_2(g) + \frac{2x + y - 2z - 2a + 2b}{6}CH_4(g) + \frac{4x - y + 2z + 2a - 8b}{6} \\ CO(g) + b\ CO_2(g)\ \Delta H &= [(485.44 + 12 * LHV)x + (101.225 + LHV)y - (202.45 - 16 * LHV)z + 83.39a - 80.54b)\ ]kJ/mol \\ &= (892.24x + 204.225y - 376.85z + 83.39a - 80.54b)\ kJ/mol\end{aligned} \quad (16)$$

The coefficient a and b represented the mole production of H_2 and CO_2 per mole of sample, respectively. H_2 and CO_2 contained most of the mole production of gasification.

At the reaction condition whose temperature was T °C and pressure was P MPa, heat absorption of the reaction could be calculated by Hess's law. The thermochemical equation was as follow:

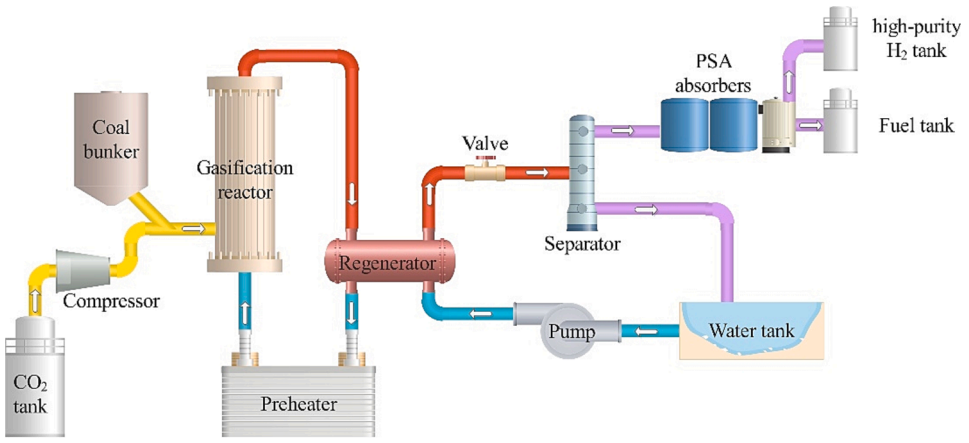

Fig. 1. Structure of the gasification system.

$$C_xH_yO_z(s) + \frac{4x - y - 4z + 2a + 4b}{6} H_2O(sc) \xrightarrow{T\ ^{\circ}C;\ P\ MPa} aH_2(sc) + \frac{2x + y - 2z - 2a + 2b}{6} CH_4(sc) + \frac{4x - y + 2z + 2a - 8b}{6} CO(sc) + b\ CO_2(sc)$$

$$\begin{aligned}\Delta H = [&-a^*(h_{T,P,H_2} - h_{25,0.1,H_2}) - \frac{2x + y - 2z - 2a + 2b}{6}*(h_{T,P,CH_4} - h_{25,0.1,CH_4}) - \frac{4x - y + 2z + 2a - 8b}{6}*(h_{T,P,CO} - h_{25,0.1,CO}) - b^*(h_{T,P,CO_2} - h_{25,0.1,CO_2}) \\ &+(892.24x + 204.225y - 376.85z + 83.39a - 80.54b) \\ &+(h_{T,P,sample} - h_{25,0.1,sample}) + \frac{4x - y - 4z + 2a + 4b}{6}(h_{T,P,H_2O} - h_{25,0.1,H_2O})]\ \text{kJ/mol}\end{aligned} \quad (17)$$

$$HE = \frac{4x + 2y - 4z + 2a + 4b}{3y} \quad (18)$$

The increase of mole fraction of C element (x) of the sample could make the increase of carbon-containing products, especially the production of CO_2 (b). As a result, the consumption of H_2O in the reactants decreased while the production of CH_4 and CO_2 increased. Meanwhile, the increase of mole fraction of H element (y) could also lead to the increase of H_2 production (a). And the production of H_2 increased with it.

3.2. The influence of temperature and pressure on gas production

The mass of each substances reacted or produced in the gasification of each temperature and pressure was shown in Table 2. It showed that mass flow of H_2, CO and CO_2 increased with temperature and decreased with pressure. That of CH_4 had the contrary trend. At low temperature, heat absorption of the reaction was at negative value and this data increased with more heat absorbed at high temperature. At 800 °C, the heat absorption reached 61.10 kW.

Steam reforming reaction (6) was the most crucial reaction as mentioned, so the products of steam reforming reaction, H_2 and CO_2, became the main mole products of the gasification and the gasification

Table 2
Consumption and production of gasification at different temperature and pressure.

Temperature (°C)	Pressure (MPa)	Reactants (kg/h)		Products (kg/h)				Reaction heat (kW)	HE (%)
		Lignite	H_2O	H_2	CH_4	CO	CO_2		
600	23	100	16.79	3.98	19.54	2.53	90.74	−6.87	119.68
625	23	100	19.91	4.74	17.89	3.46	93.82	0.64	124.42
650	23	100	23.20	5.56	16.09	4.63	96.91	10.28	129.41
675	23	100	26.57	6.42	14.18	6.06	99.92	17.37	134.55
700	23	100	38.79	7.30	12.19	7.75	102.70	26.34	139.68
725	23	100	33.19	8.17	10.19	9.70	105.13	35.47	144.62
750	23	100	36.18	8.99	8.24	11.87	107.09	44.51	149.17
775	23	100	38.79	9.74	6.42	14.17	108.47	53.15	153.15
800	23	100	40.91	10.38	4.80	16.51	109.21	61.10	156.37
650	23	100	23.20	5.56	16.09	4.63	96.91	10.28	129.41
650	25	100	22.12	5.31	16.63	4.44	95.74	6.97	127.78
650	27	100	21.13	5.08	17.11	4.28	94.67	5.36	126.28
650	29	100	20.23	4.86	17.56	4.13	93.68	3.88	124.91

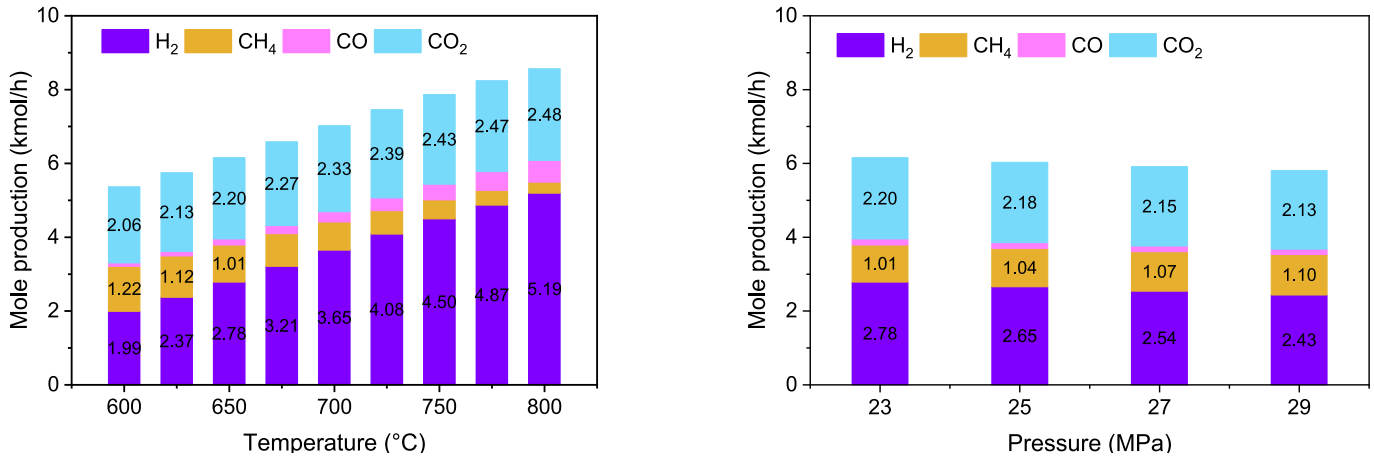

Fig. 2. Influence of (A) Temperature and (B) Pressure on the mole production of each substance.

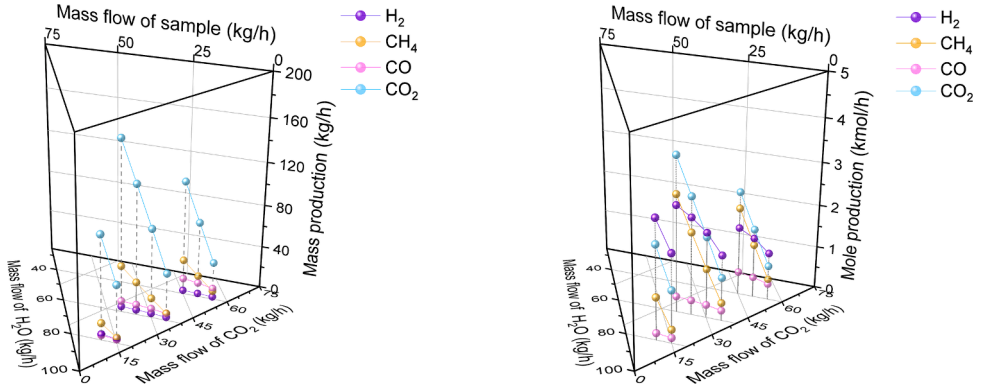

Fig. 3. The production at different input ratio of each substance (A) mass production; (B) mole production (650 °C, 23 MPa).

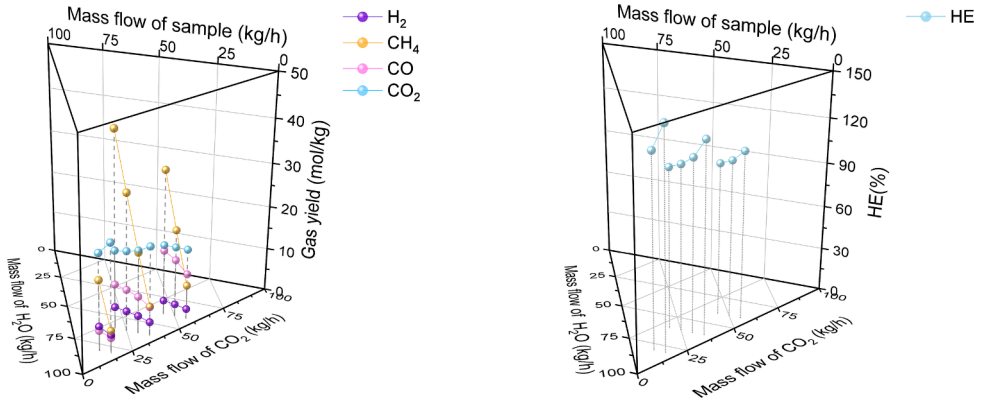

Fig. 4. (A) Yields of gas products and (B) HE at different input ratio.

reaction was mainly the endothermic reaction in this research which was because the value of heat released by methanation reaction (8) was lower than the value of heat absorbed by other reactions at high temperature. CO was produced by H_2 and CO_2 in the reverse reaction of water–gas shift reaction (7) and CH_4 was produced in methanation reaction (8). High temperature would promote the endothermic reactions such as the steam reforming reaction (6) and the reverse reaction of water–gas shift reaction (7), and it could also inhibit the exothermic reactions such as methanation reaction (8). As a result, production of H_2, CO and CO_2 increased while that of CH_4 decreased with temperature. In addition, heat absorption of the total reaction increased. It could also explain the fact that methanation reaction (8) released more heat at low temperature and the heat absorption of gasification reaction was negative. Summary of mole coefficients of gas products was higher than that of gas reactants in steam reforming reaction (6), which meant that steam reforming reaction (6) was inhibited by pressure. Meanwhile, methanation reaction (8) was promoted as well. The reaction heat absorption also decreased with pressure. Total mass production of the products equalled the mass consumption of reactants which increased with temperature and decreased with pressure. Gasification reaction was an endothermic reaction at high temperature and promoted at high temperature. Heat absorption of the reaction also increased as shown in

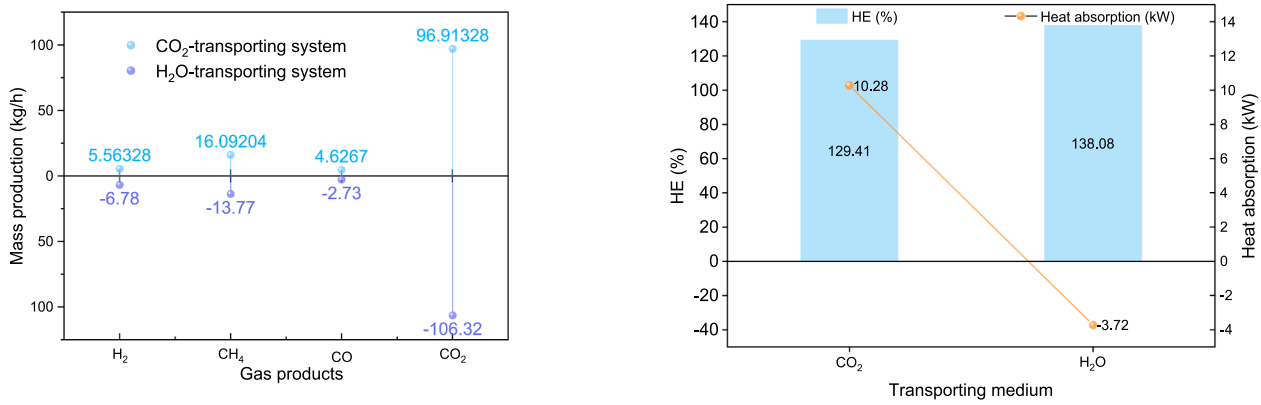

Fig. 5. (A) Gas production of each product and (B) HE and the heat absorption in double reactions.

Table 2. With the production of gas products, the pressure of the reactor increased and the reaction was inhibited. In addition, HE showed the conversion efficiency of H atoms. HE increased from 119.68 % at 600 °C, 23 MPa to 156.37 % at 800 °C, 23 MPa. Meanwhile, HE decreased about 1.5 % from 23 MPa to 29 MPa at 650 °C. According to the law of conservation of atoms, H atoms in products equalled those in reactants. The mass flow of feedstock was stable and HE was positively correlated with consumption of water in the reactant.

Fig. 2 showed the influence on mole production of the substances. It was obvious that the mole production of CO increased and that of CH_4 decreased with temperature. Meanwhile, mole production of H_2 increased sharply and that of CO_2 also increased. The mole production of H_2 per mol of lignite increased more than that of CO_2 with temperature, which caused the increase of (a-b) in (17). Moreover, the mole production of CH_4 decreased and that of CO increased.

3.3. The influence of the ratio of H_2O, CO_2 and lignite on gas production

In previous researches on supercritical gasification, the feedstock concentration was no more than 25 % [39–42]. Then the mass ratio of H_2O and lignite in this paper was no less than 3:1. Meanwhile, the solid phase volume fraction of supercritical CO_2 transporting cutting was always no more than 10 vol% [28,30,43–45]. The density of CO_2 at 650 °C and 23 MPa was 124.32 kg/m^3 and the density of lignite was about 1450–1800 kg/m^3 [46,47]. The mass ratio of CO_2 and lignite in this paper was no less than 1:1.

Fig. 3 showed the gas production at different ratios of H_2O, CO_2 and lignite. Each gas production increased with the mass flow of lignite. At low concentration of lignite, H_2 and CO_2 was the main mole products. Meanwhile, the mole fraction of CH_4 contained no more than 15 mol% when the lignite concentration was lower than 10 wt%. Mole fraction of CH_4 increased sharply at high lignite concentration and reached 22.27 mol% at the ratio equaled 8:9:3. The production of H_2, CH_4 and CO_2 increased with the concentration of sample when one of the proportion of H_2O or CO_2 input was kept constant.

The gas yield was shown in Fig. 4, the yields of H_2, CH_4 and CO_2 increased with the proportion of lignite, especially the yield of CH_4. Yield of CO decreased with the mass flow of lignite. Moreover, yield of CO increased with the proportion of CO_2 input while the yield of CO_2 decreased.

Free radical reactions were dominant over ionic reactions in supercritical water [48]. As mentioned above, supercritical water played as a source of H and free radicals [13]. The decrease of water or the increase of lignite meant less H and free radicals provided by supercritical water per kilogram of lignite. The yield of H_2 decreased [15]. In addition, the increase of CO_2 inhibited the yield of CO_2 according to Le Chatelier's principle. In conclusion, the decrease of water or the increase of lignite made the coefficient (a) in (17) decrease and the the increase of CO_2 made the coefficient (b) decrease. When the coefficient (a) increased faster than (b), the yield of CH_4 decreased while that of CO increased. HE also increased with the H and free radicals provided by supercritical water per lignite increment, decreased with the decrease of water or the increase of lignite inhibited as mentioned.

3.4. The influence of transporting medium on gas production

The H_2O-transporting system was used to compare with the CO_2-transporting system and the influence of transporting medium was investigated. Parameters such as the reaction temperature, pressure, the ratio of H_2O, transporting medium and lignite in the H_2O-transporting

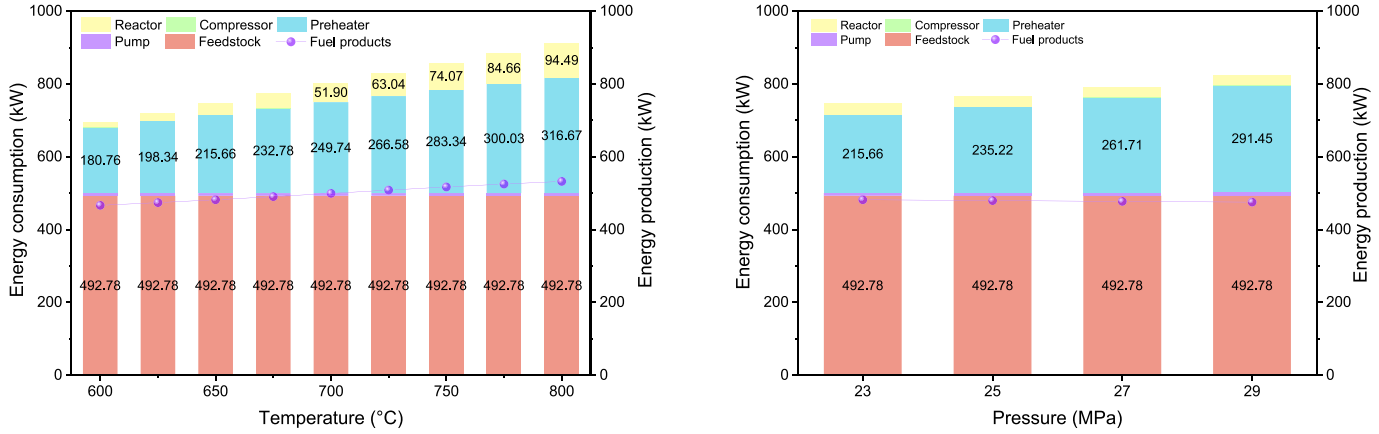

Fig. 6. The energy consumption and production at (A) different temperature; (B) different pressure.

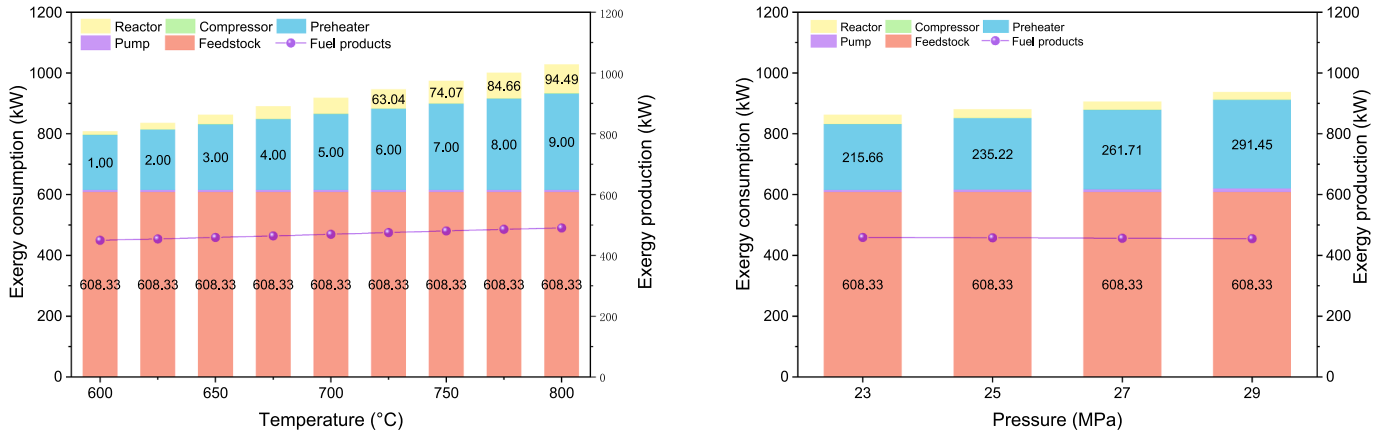

Fig. 7. The exergy consumption and production at (A) different temperature; (B) different pressure.

system were in the same range. Fig. 5 showed the production of both systems. With extra CO_2 input into the CO_2-transporting system, the reaction equilibrium shifted to the direction of weakening CO_2, which meant part of H_2 in the products was used to reduce CO_2. As a result, the products of the system contained less H_2 and CO_2 and the production of CH_4 and CO increased. The production of H_2, CH_4, CO, CO_2 were 5.56 kg/h, 16.09 kg/h, 4.63 kg/h and 96.91 kg/h in CO_2-transporting system while the production in H_2O-transporting system was 6.78 kg/h, 13.77 kg/h, 2.73 kg/h and 106.31 kg/h. HE in the system transported by CO_2 and H_2O were 129.41 % and 138.08 %. Heat absorption of CO_2-transporting system was 8.75 kW.

The change of transporting medium from H_2O to CO_2 meant more CO_2 and less H_2O input into the system, which could inhibit the gasification reaction according to Le Chatelier's principle. As a result, the production and HE decreased. Heat absorption of the reaction also decreased. (17) could also tell the trend. The mole production of total products was (a + x), which increased with the yield of H_2 linearly. The changed caused less H_2 and the coefficient (a) of H_2 in (17). Then the total production decreased. HE decreased with both (a) and (b) shown in (18). In conclusion, the change from H_2O to CO_2 inhibited the reaction.

4. Energy and exergy analysis of the gasification system

4.1. Energy and exergy analysis in different temperature and pressure

It was obvious that the energy consumption increased with both temperature and pressure shown in Fig. 6. The mass flow of lignite was same and the input of feedstock was stable. Energy consumption in pump and compressor was negligible. Therefore, the analysis of energy consumption in preheater and reactor was the key of the energy input in the whole system.

The output water from regenerator was at 400 °C and the heat consumption of preheater was used to heat the water from 400 °C to reaction temperature. The specific heat capacity of supercritical phase decreased with temperature slightly [49]. The heat consumption increased almost linear and the difference between adjacent temperature range decreased slightly.

In addition, the energy consumption in reactor could be divided into three parts, energy to heat the feedstock (CO_2 and lignite), the heat absorption of gasification reaction and the energy loss of the reactor. The first part to heat feedstock was similar as the energy consumption of preheater which increased with temperature. The gasification reaction was an endothermic reaction as shown in Table 2, which absorbed much heat at high temperature. Therefore, the second part increased with temperature as well. High temperature meant high temperature difference with the environment and high temperature difference caused much energy loss. In conclusion, energy consumption increased with temperature.

As for pressure, the difference of specific heat capacity increased with pressure [50]. So the energy consumption of preheater also increased. It was found that gasification reaction was inhibited with pressure shown in Fig. 2, which resulted in the decrease of energy consumption in reactor although the energy consumption to heat feedstock increased.

Energy production approximately equaled the energy of gasification products at standard condition. In (16), heat absorption at standard

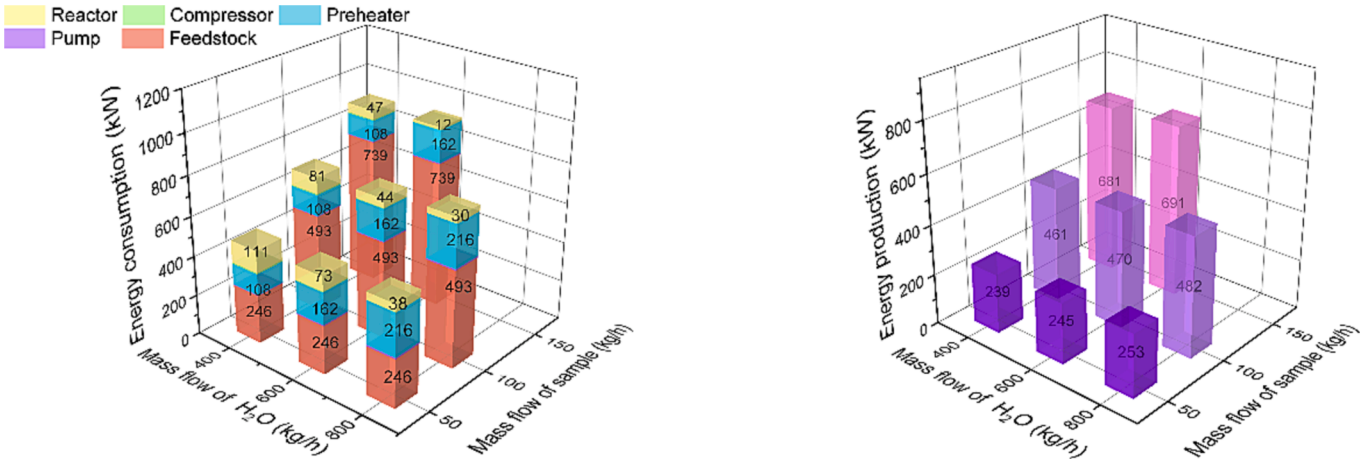

Fig. 8. The energy (A) consumption and (B) production at different mass flow of H_2O and lignite.

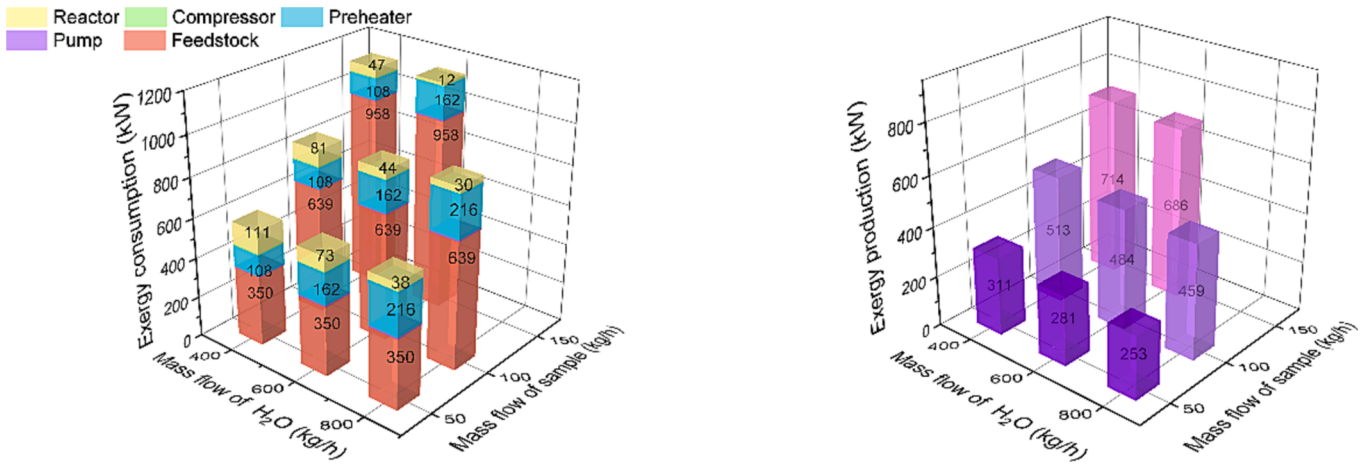

Fig. 9. The exergy (A) consumption and (B) production at different mass flow of H_2O and lignite.

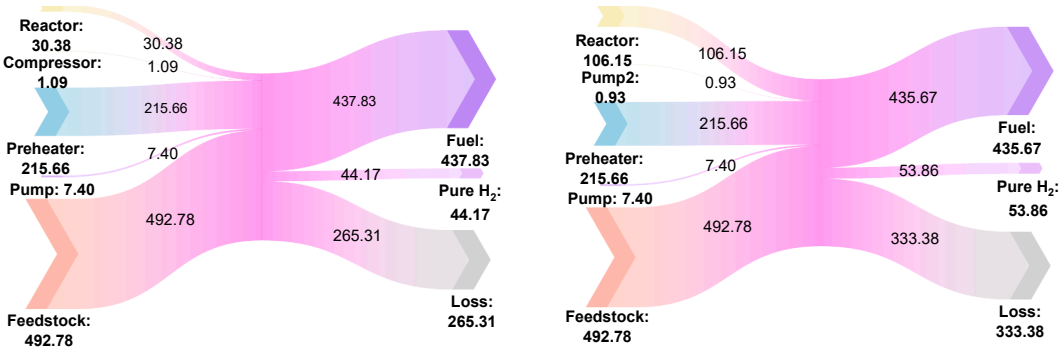

Fig. 10. Energy flow of (A) CO_2-transporting system and (B) H_2O-transporting system.

condition increased with (83.39*a*-80.54*b*). As shown in Fig. 2, the mole production of H_2 increased much faster than that of CO_2 with temperature and (83.39*a*-80.54*b*) increased as well. As a result, the heat absorption at standard condition increased. According to the law of conservation of energy, the energy of products equaled the summary of the energy of reactants and heat absorption. Energy of reactants equaled the chemical energy of lignite. Therefore, energy production of the system increased with temperature. Meanwhile, the mole production of H_2 and CO_2 had similar growth trends, which resulted in the slight decrease of energy production.

The exergy consumption of each module was same as the energy consumption. The chemical exergy of lignite was used the modifier formula in previous research [24,51]. The results of exergy were shown in Fig. 7. The trend of exergy consumption was similar with that of energy consumption while the exergy production was lower than energy production. The increasing trend of exergy production was also slower than that of energy production due to more loss in the form of heat.

4.2. *Energy and exergy analysis at different ratio of H_2O, CO_2 and lignite*

The energy consumption and production of the system increased with both lignite and H_2O as shown in Fig. 8 (A). Energy in feedstock was proportional to the mass flow of lignite while the energy consumption of pump and preheater also was proportional to the mass flow of H_2O. Energy to heat feedstock was influenced by the mass flow of CO_2 and that of lignite. Gasification reaction was promoted by the increase of H_2O and lignite. Heat loss of reactor was influenced slightly by feedstock concentration. Finally, the energy in feedstock only increased with

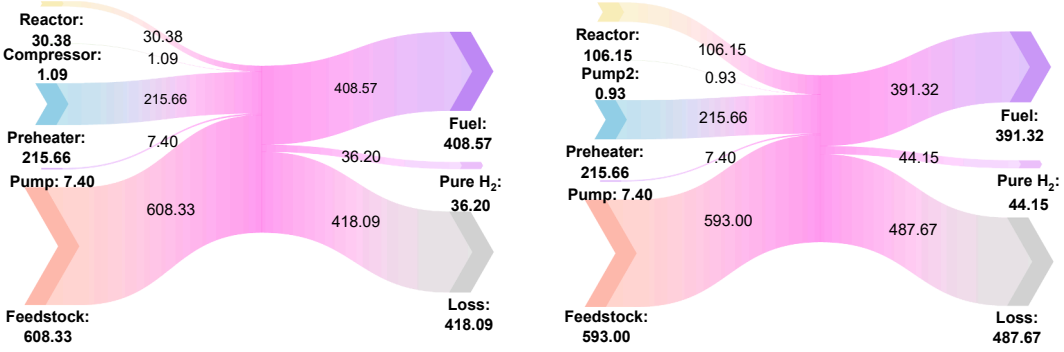

Fig. 11. Exergy flow of (A) CO_2-transporting system and (B) H_2O-transporting system.

lignite sharply and energy consumption only increased with H_2O sharply. The energy consumption of reactor decreased with both lignite and H_2O. The total energy consumption increased with both lignite and H_2O under the combined influence.

Energy production was affected by the production of gas products. All the products increased with the mass flow of lignite. The increase of CO_2 and decrease with H_2O inhibited the gasification reaction. As a result, the energy production increased with H_2O and decreased with CO_2.

Consumption and production of exergy in the system showed same trend with those of energy, as shown in Fig. 9. Exergy input changed in the range of 578.93 kW to 1140.52 kW. The main input into the system was the chemical exergy in feedstock, containing more than 60 % of the total input. The exergy production of the system had an increase of about 200 kW when the increase of lignite mass flow was 50 kg/h and an increase of 25 kW when the increase of H_2O mass flow equaled 200 kg/h.

4.3. Energy and exergy analysis in the systems with different transporting mediums

Energy flow of both systems were shown in Fig. 10. Energy consumption in reactor, preheater and energy in feedstock was the main input of the system and the energy in fuel and pure H_2 was the main products of the system. In addition, some energy released to the environment in the form of heat.

As mentioned before, the energy consumption was only influenced by the mass flow of main water flow. And the values in both systems were same. Energy to heat feedstock was less with CO_2 transporting due to the low critical point and specific heat capacity of CO_2. CO_2 inhibited the gasification reaction while H_2O promoted it, according to Le Chatelier's principle. As a result, the reaction would absorb more heat in H_2O-transporting system. Heat loss in H_2O-transporting system was also higher than that in CO_2-transporting system. In conclusion, H_2O-transporting system had more energy consumption in reactor than CO_2-transporting system. So the total energy input into the H_2O-transporting system was high.

As shown in Fig. 5, H_2O-transporting system produced more H_2 while the CO_2-transporting system produced more CH_4. It resulted in more energy contained in pure H_2 in H_2O-transporting system while fuel gas in CO_2-transporting system contained more chemical energy. The total energy consumption was 482.00 kW (CO_2-transporting system) and 489.54 kW (H_2O-transporting system), contrastively.

Much more energy was input into the H_2O-transporting system but the energy productions were similar. Therefore, the H_2O-transporting system had low energy efficiency and high energy loss. The energy efficiency of the H_2O-transporting system was 59.49 % while that of CO_2-transporting system was 64.61 %. The energy loss of the H_2O-transporting system equaled 333.38 kW while that of CO_2-transporting system was 264.06 kW. It proved that system with CO_2 transporting had ability to save the energy.

Exergy flows were same in both systems shown in Fig. 11. It was obvious that the main exergy input was still reactor, preheater and the exergy in feedstock. The two parts of exergy output were lower than energy production while the exergy loss was higher than energy loss. The exergy input of CO_2-transporting system was 862.87 kW while that of H_2O-transporting system was 923.14 kW. Exergy output was 444.77 kW and 435.47 kW, contrastively. The system with H_2O transporting caused more exergy input and obtained less exergy output, resulting in its low exergy efficiency. On the other hand, the exergy loss of CO_2-transporting was 418.09 kW, much lower than that of H_2O-transporting system which equaled 487.67 kW.

5. Conclusion

This paper established a coal supercritical gasification system and Yimin lignite was selected as the sample. The influence of reaction condition such as temperature, pressure and feedstock concentration on gas production was investigated. In addition, energy and exergy consumption in the gasification system was also researched. The results were as follows:

(1) Mass flow of H_2, CO and CO_2 increased with temperature and decreased with temperature. That of CH_4 had the contrary trend. Mole production of CO increased from 0.09 kmol/h to 0.58 kmol/h and that of CH_4 decreased from 1.22 kmol/h to 0.30 kmol/h with temperature. Meanwhile, mole production of H_2 increased sharply from 1.99 kmol/h to 5.19 kmol/h and that of CO_2 also increased about 0.42 kmol/h.
(2) Each gas production increased with feedstock concentration. The yields of H_2, CH_4 and CO_2 increased with lignite while yield of CO decreased. Yields of H_2, CH_4, CO and CO_2 were 30.95 mol/kg, 8.43 mol/kg, 4.76 mol/kg and 20.44 mol/kg when feedstock concentration was 5 wt%. The yields reached 12.57 mol/kg, 13.80 mol/kg, 1.85 mol/kg and 18.10 mol/kg at 20 wt% feedstock concentration.
(3) Energy and exergy input into the system increased with both temperature and pressure. They also increased with the mass flow of both lignite and H_2O. Energy and exergy input increased from 693.10 kW and 808.65 kW at 600 °C to 912.43 kW and 1027.99 kW at 800 °C, respectively. Energy and exergy production increased from 466.56 kW and 449.96 kW at 23 MPa to 532.27 kW and 490.44 kW at 29 MPa, respectively. Energy input changed in the range of 475.16 kW to 921.19 kW with the mass flow of different input. Energy production increased with mass flow of lignite and H_2O and decreased with that of CO_2. Exergy input increased from 578.93 kW to 1140.52 kW and exergy production increased in the range of 252.91 kW to 714.05 kW.
(4) H_2O-transporting system had high energy and exergy input and low exergy obtained. Energy production of H_2O-transporting system was higher than energy production of CO_2-transporting system but the difference between the production was no more than 1.5 %. Energy and exergy efficiency of CO_2-transporting system were 64.61 % and 53.04 %, respectively. And those of H_2O-transporting system were 59.49 % and 48.42 %, respectively.

Declaration of Competing Interest

The authors declare that they have no known competing financial interests or personal relationships that could have appeared to influence the work reported in this paper.

Data availability

Data will be made available on request.

Acknowledgment

This work is supported by the Basic Science Center Program for Ordered Energy Conversion of the National Natural Science Foundation of China (No.51888103).

References

[1] L. Li, Y. Lei, Q. Xu, S. Wu, D. Yan, J. Chen, Crowding-out effect of coal industry investment in coal mining area: taking Shanxi province in China as a case, Environ. Sci. Pollut. Res. 24 (2017) 23290–23298.
[2] Y. Li, B. Zhang, B. Wang, Z. Wang, Evolutionary trend of the coal industry chain in China: Evidence from the analysis of I-O and APL model, Resour. Conserv. Recycl. 145 (2019) 399–410.
[3] B. Roy, A. Schaffartzik, Talk renewables, walk coal: The paradox of India's energy transition, Ecol. Econ. 180 (2021), 106871.
[4] W. Suwala, Modelling adaptation of the coal industry to sustainability conditions, Energy 33 (2008) 1015–1026.

[5] W. Wang, B. Li, X. Yao, J. Lyu, W. Ni, Air pollutant control and strategy in coal-fired power industry for promotion of China's emission reduction, Front. Energy 13 (2019) 307–316.
[6] Y. Zhang, B. Jin, X. Zou, H. Zhao, A clean coal utilization technology based on coal pyrolysis and chemical looping with oxygen uncoupling: Principle and experimental validation, Energy 98 (2016) 181–189.
[7] J. Chen, L. Wang, Z. Cheng, L. Lu, L. Guo, H. Jin, D. Zhang, R. Wang, S. Liu, Performance simulation and thermodynamics analysis of hydrogen production based on supercritical water gasification of coal, Int. J. Hydrogen Energy 46 (2021) 28474–28485.
[8] A. Chavda, P. Mehta, A. Harichandan, Numerical analysis of multiphase flow in chemical looping reforming process for hydrogen production and CO2 capture, Exp. Computat. Multiphase Flow 4 (2022) 360–376.
[9] L.-S. Fan, L. Zeng, W. Wang, S. Luo, Chemical looping processes for CO2 capture and carbonaceous fuel conversion – prospect and opportunity, Energ. Environ. Sci. 5 (2012) 7254–7280.
[10] Y. Wang, H. Wang, H. Jin, Direct Numerical Simulation of Fluid Flow and Heat Transfer of a Reactive Particle Layer with Stefan Flow in Supercritical Water, Ind. Eng. Chem. Res. 62 (2023) 1636–1645.
[11] M. Recalde, A. Amladi, V. Venkataraman, T. Woudstra, P.V. Aravind, Thermodynamic analysis of supercritical water gasification combined with a reversible solid oxide cell, Energ. Conver. Manage. 270 (2022), 116208.
[12] X. Chen, Z.F. Tian, P.J. van Eyk, D. Lewis, G.G.J. Nathan, Numerical simulation of hydrothermal liquefaction of algae in a lab-scale coil reactor, Exp. Computat. Multiphase Flow 4 (2022) 113–120.
[13] K.C. Park, H. Tomiyasu, Gasification reaction of organic compounds catalyzed by RuO2 in supercritical water, Chem. Commun. (2003) 694–695.
[14] Y. Guo, S.Z. Wang, D.H. Xu, Y.M. Gong, H.H. Ma, X.Y. Tang, Review of catalytic supercritical water gasification for hydrogen production from biomass, Renew. Sustain. Energy Rev. 14 (2010) 334–343.
[15] Y. Hu, M. Gong, X. Xing, H. Wang, Y. Zeng, C.C. Xu, Supercritical water gasification of biomass model compounds: A review, Renew. Sustain. Energy Rev. 118 (2020), 109529.
[16] A. Kruse, E. Dinjus, Hot compressed water as reaction medium and reactant: Properties and synthesis reactions, J. Supercrit. Fluids 39 (2007) 362–380.
[17] X. Li, H. Wang, Y. Li, H. Jin, Effects of physical properties of supercritical water on coarse graining of particle cluster, Particuology 82 (2023) 166–178.
[18] J. Chen, Y. Liu, X. Wu, E J., E. Leng, F. Zhang, G. Liao, Thermodynamic, environmental analysis and comprehensive evaluation of supercritical water gasification of biomass fermentation residue, J. Clean. Prod. 361 (2022) 132126.
[19] Z. Chen, L. Gao, X. Zhang, W. Han, S. Li, High-efficiency power generation system with integrated supercritical water gasification of coal, Energy 159 (2018) 810–816.
[20] A. Nurdiawati, I.N. Zaini, A.R. Irhamna, D. Sasongko, M. Aziz, Novel configuration of supercritical water gasification and chemical looping for highly-efficient hydrogen production from microalgae, Renew. Sustain. Energy Rev. 112 (2019) 369–381.
[21] H. Ke, T. Li-hua, Z. Zi-bin, Z. Cheng-fang, Reaction mechanism of styrene monomer recovery from waste polystyrene by supercritical solvents, Polym. Degrad. Stab. 89 (2005) 312–316.
[22] H. Zhong, Z. Wei, Y. Man, S. Pan, J. Zhang, B. Niu, X. Yu, Y. Ouyang, Q. Xiong, Prediction of instantaneous yield of bio-oil in fluidized biomass pyrolysis using long short-term memory network based on computational fluid dynamics data, J. Clean. Prod. 391 (2023), 136192.
[23] R. Mu, M. Liu, J. Yan, Advanced exergy analysis on supercritical water gasification of coal compared with conventional O2–H2O and chemical looping coal gasification, Fuel Process. Technol. 245 (2023), 107742.
[24] W. Wang, C. Wang, Y. Huang, H. Lu, J. Chen, J. Shi, H. Jin, Heat, Electricity, and Fuel Gas Ploy-Generation System on an Island based on Plastic Waste Gasification in Supercritical Water, ACS Sustain. Chem. Eng. 10 (2022) 13786–13791.
[25] J. Ni, L. Qian, Y. Wang, B. Zhang, H. Gu, Y. Hu, Q. Wang, A review on fast hydrothermal liquefaction of biomass, Fuel 327 (2022), 125135.
[26] L. Mao, B. Lu, J. Shi, Y. Zhang, X. Kang, Y. Chen, H. Jin, L. Guo, Rapid high-temperature hydrothermal post treatment on graphitic carbon nitride for enhanced photocatalytic H2 evolution, Catal. Today 409 (2023) 94–102.
[27] L. Hou, T. Jiang, H. Liu, X. Geng, B. Sun, G. Li, S. Meng, An evaluation method of supercritical CO2 thickening result for particle transporting, J. CO2 Util. 21 (2017) 247–252.
[28] Z.-G. He, G.-S. Li, H.-Z. Wang, Z.-H. Shen, S.-C. Tian, P.-Q. Lu, B. Guo, Numerical simulation of the abrasive supercritical carbon dioxide jet: The flow field and the influencing factors, Journal of Hydrodynamics, Ser. B 28 (2016) 238–246.
[29] B. Sun, J. Wang, Z. Wang, Y. Gao, J. Xu, Calculation of proppant-carrying flow in supercritical carbon dioxide fracturing fluid, J. Pet. Sci. Eng. 166 (2018) 420–432.
[30] L. Hou, X. Bian, X. Geng, B. Sun, H. Liu, W. Jia, Incipient motion behavior of the settled particles in supercritical CO2, J. Nat. Gas Sci. Eng. 68 (2019), 102900.
[31] Y. Zheng, H. Wang, G. Tian, M. Liu, G. Li, E. Kuru, Experimental investigation of proppant transport in hydraulically fractured wells using supercritical CO2, J. Pet. Sci. Eng. 217 (2022), 110907.
[32] K. Jiang, J. Shi, Q. Zhao, H. Jin, Research progress of industrial application based on two-phase flow system of supercritical carbon dioxide and particles, Powder Technol. 407 (2022), 117621.
[33] C. Wang, H. Jin, C. Fan, K. Luo, S. Guo, Exergy and energy analysis of coal gasification in supercritical water with external recycle system, Int. J. Chem. React. Eng. 17 (2019) 20190010.
[34] W. Liemberger, M. Groß, M. Miltner, M. Harasek, Experimental analysis of membrane and pressure swing adsorption (PSA) for the hydrogen separation from natural gas, J. Clean. Prod. 167 (2017) 896–907.
[35] P. Brea, J.A. Delgado, V.I. Águeda, M.A. Uguina, Comparison between MOF UTSA-16 and BPL activated carbon in hydrogen purification by PSA, Chem. Eng. J. 355 (2019) 279–289.
[36] L. Wang, J. Chen, J. Cui, G. Wang, H. Jin, L. Guo, Experimental study on treatment of mixed ion exchange resins by supercritical water gasification, J. Clean. Prod. 385 (2023), 135755.
[37] C. Yang, S. Wang, Y. Li, Y. Zhang, C. Cui, Thermodynamic analysis of hydrogen production via supercritical water gasification of coal, sewage sludge, microalga, and sawdust, Int. J. Hydrogen Energy 46 (2021) 18042–18050.
[38] J. Xu, Z. Peng, S. Rong, H. Jin, L. Guo, X. Zhang, T. Zhou, Model-based thermodynamic analysis of supercritical water gasification of oil-containing wastewater, Fuel 306 (2021), 121767.
[39] A.B.A. Ibrahim, H. Akilli, Supercritical water gasification of wastewater sludge for hydrogen production, Int. J. Hydrogen Energy 44 (2019) 10328–10349.
[40] J. Chen, W. Xu, F. Zhang, H. Zuo, E J., K. Wei, G. Liao, Y. Fan, Thermodynamic and environmental analysis of integrated supercritical water gasification of coal for power and hydrogen production, Energy Convers. Manage. 198 (2019) 111927.
[41] K. Babaei, A. Bozorg, A. Tavasoli, Hydrogen-rich gas production through supercritical water gasification of chicken manure over activated carbon/ceria-based nickel catalysts, J. Anal. Appl. Pyrol. 159 (2021), 105318.
[42] P. Liu, W. Wei, Q. Zhao, J. Shi, B. Bai, H. Jin, Visualization of polyoxymethylene (POM) particle decomposition behavior in hydrothermal condition, Therm. Sci. Eng. Progress (2023), 101825.
[43] Z. Shen, H. Wang, G. Li, Numerical simulation of the cutting-carrying ability of supercritical carbon dioxide drilling at horizontal section, Pet. Explor. Dev. 38 (2011) 233–236.
[44] Y. Zheng, H. Wang, B. Yang, Y. Hu, Z. Shen, H. Wen, W. Yan, CFD-DEM simulation of proppant transport by supercritical CO2 in a vertical planar fracture, J. Nat. Gas Sci. Eng. 84 (2020), 103647.
[45] X.-Z. Song, G.-S. Li, B. Guo, H.-Z. Wang, X.-J. Li, Z.-H. Lü, Transport feasibility of proppant by supercritical carbon dioxide fracturing in reservoir fractures, J. Hydrodyn. 30 (2018) 507–513.
[46] J. Wang, Y. He, Y. Zhang, X. Zhao, Z. Peng, S. Wang, T. Zhang, Research on cationic surfactant adsorption performance on different density lignite particles by XPS nitrogen analysis, Fuel 213 (2018) 48–54.
[47] J. Wang, Y. He, X. Ling, J. Hao, W. Xie, Adsorption Performance of Nonionic Surfactant on the Lignite Particles with Different Density, Energy Fuel 31 (2017) 6580–6586.
[48] M.D. Bermejo, M.J. Cocero, Supercritical water oxidation: A technical review, AIChE J 52 (2006) 3933–3951.
[49] HuiJin, Yingdong Wang, Huibo Wang, Zhenqun Wu, Xiao yuLi, Influence of Stefan flow on the drag coefficient and heat transfer of a spherical particle in a supercritical water cross flow, Phys. Fluids 33 (2021) 023313.
[50] Kun Jiang, Bowei Zhang, Weizuo Wang, Hui Jin, Effect of the variable physical properties on sub- and supercritical CO2 flowing over a stationary spherical particle, Phys. Fluids 34 (2022) 103605.
[51] H. Jin, C. Wang, C. Fan, Simulation Study on Hydrogen-Heating-Power Poly-Generation System based on Solar Driven Supercritical Water Biomass Gasification with Compressed Gas Products as an Energy Storage System, J. Therm. Sci. 29 (2020) 365–377.